Xingyu Fu[1,2]
Department of Mechanical Engineering,
Purdue University,
West Lafayette, IN 47906
e-mail: fu237@purdue.edu

Fengfeng Zhou[2]
Department of Mechanical Engineering,
Purdue University,
West Lafayette, IN 47906
e-mail: zhou966@purdue.edu

Huitaek Yun
Department of Mechanical Engineering,
Purdue University,
West Lafayette, IN 47906
e-mail: yun37@purdue.edu

Eunseob Kim
Department of Mechanical Engineering,
Purdue University,
West Lafayette, IN 47906
e-mail: kim3235@purdue.edu

Siying Chen
Department of Mechanical Engineering,
Purdue University,
West Lafayette, IN 47906
e-mail: chen2122@purdue.edu

Martin Byung-Guk Jun
Department of Mechanical Engineering,
Purdue University,
West Lafayette, IN 47906
e-mail: mbgjun@purdue.edu

Machine Straightness Error Measurement Based on Optical Fiber Fabry–Pérot Interferometer Monitoring Technique

In this research, we propose an Error Separation Technique (EST) based on optical fiber sensors for on-machine straightness error measurement. Two fiber optic Fabry–Pérot interferometers have been developed serving as two displacement sensors. The displacement distance is computed according to the reflected spectrum from interferometers, which can achieve a sub-micrometer resolution. The two-point method has been employed to separate the straightness error of the slides and the profile error of a fine-polished standard block. The spacing distance between two interferometers is determined by the diameter of optical fibers so that the EST's resolution has the potential to reach the sub-millimeter scale. In the experiment, the straightness error has been measured on a commercially available computer numerical control machine tool, and the measurement has been conducted on its x-axis. The spacing distance between two optical fiber sensors is 1.5 mm which equals the EST's resolution along the machine tool's x-axis. The separated profile error of the measured standard block is around 30 μm which has been verified by a high precision Coordinate Measurement Machine (CMM). The magnitude of the separated straightness error is around 40 μm. This technique is flexible and simple to be conducted, which can contribute to the micro-machine tool calibration and other straightness error applications.
[DOI: 10.1115/1.4055897]

Keywords: error separation technique (EST), fiber optic Fabry–Pérot interferometer, straightness measurement, metrology, sensing, monitoring and diagnostics

1 Introduction

Nowadays, the evaluation of the machine tool's accuracy becomes important due to the increasing demand for precision products. However, as the key component of the machine tools, the linear slideway suffers from various errors, for instance, positioning errors, straightness errors, and angular errors caused by yawing/pitching/rolling. From these errors, the positioning error can be compensated by the efficient closed-loop controller and the precision encoder. The angular errors usually can be converted into the straightness error when the second-order term is omitted. Therefore, the straightness error becomes a crucial indicator of the overall slide's accuracy and the machine tool's precision.

Many researchers have investigated the straightness measurement of the slide. A widely acknowledged way to evaluate the straightness error is by using a laser interferometer [1]. However, this method usually requires conducting the measurement offline and sometimes needs removing the machine tool's shell cover to expose the slides for the building of the optical path. A precision laser interferometer is not cost-efficient. Also, offline straightness measurement can involve large alignment error that comes from the difference between the measurement coordinate and the machine tool's coordinate. These drawbacks call for a simple on-machine straightness measurement using only displacement sensors, which leads to the development of the Error Separation Technique (EST).

The EST usually uses several probes to measure the surface of the slide first and then decouples the straightness errors of the slide from the profile errors of the slide surface. This method is not only applied to measure the slide straightness error but also employed to execute precision measurements when the straightness error has the same magnitude as the profile error. The first EST was used to measure the roundness error of the spindle [2] and then improved to measure the straightness error of the slides [3]. The two-point method is one of the most representative EST approaches which only requires two displacement sensors to measure the slide on the machine simultaneously. The basic form of the two-point method is the Sequential Two Point (STP) [3] (also called the inclination method [4,5]). The sampling distance between two measurement points is determined by the spacing distance between two displacement sensors, and the diameter of the displacement sensors is usually more than or around 10 mm scale so that the resolution of the inclination method is hard to reach 1 mm scale [5–7]. This low-resolution issue not only hinders the EST's application on high-resolution straightness error measurement (e.g., micro-machine tool's calibration) but also affects the profile error measurement with some high-frequency structures (for instance, the measured part with stepwise edges).

In order to improve the resolution of the inclination method, Refs. [8,9] have proposed the Generalized Two Point method (GTP) by shifting the senor with a certain distance and using this shifting distance as the sampling distance of EST. This shifting distance can be a millimeter scale or sub-millimeter scale. However,

[1]Corresponding author.
[2]These authors contributed equally to this work.
Manuscript received June 29, 2022; final manuscript received October 2, 2022; published online October 18, 2022. Assoc. Editor: Radu Pavel.

this method is highly dependent on the repeatability of the slide error for the sensor shifting and the frequency component with periods equal to the sensors' spacing distance can be lost [5]. Later, the Combined Two Point method (CTP) has been introduced [4] using the least square method to combining STP and GTP to provide a high-resolution sampling frequency. However, this method assumes a standard area with no high-frequency components at the beginning of the measurement. This assumption can be challenged in real experiments, and the measurement precision can be affected. All the methods mentioned above use the time domain method, and some other methods use the frequency domain approach [10] to separate the straightness error with high sampling resolution. But since the profile and the straightness error are non-periodic, the non-constitution at the edge can involve the distortion caused by high-order harmonic components [6]. As the fundamental of the EST, the sampling distance of the two-point method becomes one of the largest issues for the researchers to investigate and lots of efforts have been exerted in this area [5–7] using complex algorithms to provide a high-resolution. Based on this fundamental two-point method, the three-point method [11], four-point method [12], and multiple-point methods [13] have been developed to measure more error components of the slides (for instance, yawing and pitching error) but still the complex algorithms need to be conducted if the high-resolution measurement is required. According to the discussion earlier, if the size of the displacement sensors can be largely decreased, all the low-resolution problems can be solved. The basic STP method can simply separate the straightness error with high resolution, and this method can also be applied to profile error measurement with delicate high-frequency structures. The optical fiber sensors cast light on it.

Optical fiber sensors have been widely used in industrial [14–17] and scientific research [18–21] applications due to their high sensitivity, compact size, immune to electromagnetic interference, etc. Fabry–Pérot (F–P) interferometer, consisting of two parallelly aligned partially reflecting mirrors, has a long history as a precise measuring tool. Compared with traditional methods for straightness monitoring, the sensing head can be placed close to each other as the diameter of a standard optical fiber is 125 μm. With the tapering technique, the diameter can be further reduced [22–24]. Due to the constructive and destructive interference of the light between the measured surface and the fiber tip, a quasi-periodical interference spectrum can be received. According to this quasi-periodical spectrum, the distance between the fiber and the measured surface can be uniquely determined with high precision [25].

Therefore, in this paper, we propose an Error Separation Technique (EST) based on optical fiber sensors for on-machine straightness error measurement. Two fiber optic Fabry–Pérot interferometers have been developed serving as two displacement sensors, and the STP method has been employed to separate the straightness error. We summarize the contribution of this work as follows:

(1) The application of the optical fiber sensors can largely improve the resolution of EST methods along the slide moving direction and meanwhile maintains high measurement precision. The sampling distance in this work has been set to 1.5 mm and can reach the sub-millimeter scale. The final measurement resolution can reach a micrometer scale.
(2) The system errors for the STP method have been fully analyzed, and some error compensation algorithms have been introduced to provide an accurate measurement result.
(3) This method provides an alternative cost-effective approach for the straightness measurement. The price for a precision displacement sensor is similar to that for an interrogator with multiple channels, while the price for the optic fibers and other required devices is low. Since most EST employs more than two displacement sensors, this method provides a relatively low-cost solution for the straightness measurement with larger measurement ranges.

This paper is organized as follows. Section 2 introduces the mechanism of the F–P interferometer and the STP method. The error analysis has been discussed in Sec. 3 to provide theoretical support for this method. Section 4 introduces the experimental setup and the details of how the measurement has been conducted. Section 5 presents the measurement result.

2 Methods

This section mainly explains the details of our straightness measurement technique. The working mechanism of the F–P interferometer is briefly described. Then, with two F–P interferometers, the Sequential Two Point (STP) method is applied to separate the profile error and the straightness error from the interferometers' output.

2.1 Sensing Principle. The F–P interferometer is formed by two parallelly aligned partially reflecting mirrors and the space (cavity) between the mirrors. If a beam of light incident from outside of the cavity with its propagation direction perpendicular to the reflection surfaces of the two mirrors, part of the light will be reflected between the two mirrors multiple times, and the rest will transmit outside of the cavity if the absorption of the cavity and the mirrors are neglected. For coherence light, interference will occur in the cavity due to the multiple reflections. For a specific refractive index of the material (or vacuum) that fills the cavity, the interference (constructively or destructively) is determined by the length of the cavity. In this experiment, an optical fiber was used to guide the incident light to the F–P cavity and the reflected light to the interrogator. The interrogator was used to record the reflected spectrum. The optical fiber is formed by the core and the cladding. The core has a refractive index slightly higher than that of the cladding so total internal reflection can occur for the guided light. Therefore, the light can be bounded tightly inside the core of the fiber. The diameter and the refractive indices of the core and the cladding are designed so that only one mode of light can exist in the optical fiber for some specific wavelength of light. In our experiment, the wavelength range of the incident light is from 1510 nm to 1590 nm, which is in the range of C-band that has a low loss in a normal single-mode optical fiber.

Figure 1(*a*) shows a schematic drawing of the optical fiber F–P interferometer used in this experiment. Two interfaces forming the cavity shown in Fig. 1(*a*) comprise two mirrors (Mirror #1 and Mirror #2) of the F–P interferometer. The light is guided in the core before reaching the cavity. When hits the interface between the core and the air (Mirror #1), part of the light was reflected into the core, and the rest part transmits through the interface and gets into the cavity. The light inside the cavity then will be reflected by Mirror #2 and travel in the opposite direction since the propagation direction is perpendicular to Mirror #2. The back-propagating light in the cavity then hits the air–core interface again, and part of the light is reflected into the cavity, and the rest travels into the core. Therefore, the light inside the cavity bounces back and forth and interferes with itself. For those wavelengths that satisfy the constructive interference constraint, the intensity will be increased; for those wavelengths that satisfy the destructive interference, the intensity will be decreased. Therefore, the high intensity and low intensity of reflected light appear alternatively. In our experiment, Mirror #2 is the surface of a polished stainless-steel block (reference surface). It is important to polish the surface since the reflectivity of the surface can affect the finesse of the spectrum.

Figure 1(*b*) shows the reflected spectrum of a polished surface (blue) and a rough surface (orange). For both spectra, we can see the peaks and the dips appear alternatively, which agrees with the previous statement. The polishing significantly improves the

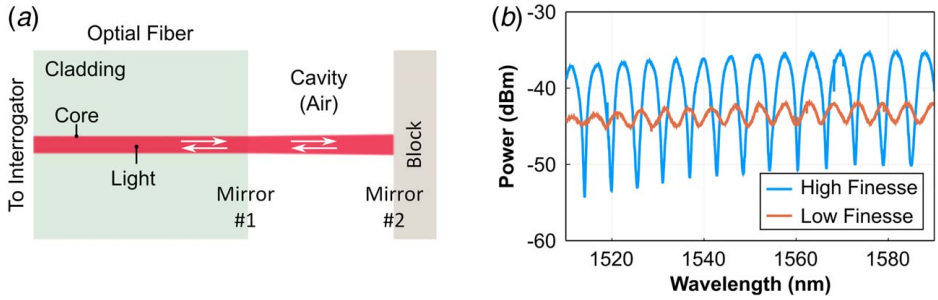

Fig. 1 Principle of the F–P cavity

finesse of the spectrum and therefore makes the analysis process easier and more reliable.

According to Ref. [25], the light reflected from the F–P cavity is

$$E_{\text{refl}} = \left(r_{12} + \frac{r_{23} t_{12} t_{21} e^{-j2\phi}}{1 - r_{21} r_{23} e^{-j2\phi}} \right) E_{\text{inc}} \tag{1}$$

where r_{12} is the reflectivity between the core of the fiber and air; r_{23} is the reflectivity of the reference surface; t_{12} is the transmissivity between the core of the fiber and air; t_{21} is the transmissivity of the air and the core; $\phi = 2\pi l_0 n_2 / \lambda_0$ is the phase change for light travels for each round inside the cavity. For example, reflected from Mirror #1 to next time reaches Mirror #1; l_0 is the distance between Mirror #1 and Mirror #2; n_2 is the material that fills the cavity (air in this experiment); λ_0 is the wavelength of the detection light in vacuum; j is the imaginary unit; E_{inc} is the electric field of the incident light. Equation (1) is a periodical function that has a period monotonically increases with the wavelength.

As introduced in Ref. [25], the average free spectrum range (FSR) was calculated using Fast Fourier Transform (FFT). However, due to the precision loss of the FFT, a scan of the cavity length was conducted to find the theoretical spectrum that matches the experimental spectrum. Therefore, the cavity length can be uniquely determined since the refractive index of air in the room environment is known.

2.2 Sequential Two Point Method. The STP method employs two displacement sensors to separate the straightness error and the measured profile. Figure 2 shows a schematic presenting the setup of the STP method. The standard block has been mounted on one side of the slide that can move along the x-axis, and two interferometers are fixed on the ground, which cannot move. Two interferometers serve as two probes: probe A and probe B to measure the distance between the standard block and the optical fibers along the y-axis. The z-axis is perpendicular to the XY plane pointing outward the paper. The raw probe outputs, $P_A(x)$ and $P_B(x)$ from probes A and B, respectively, include both the profile error $f(x)$ from the standard block and the y-axis straightness error $e_y(x)$ from the slide, where x represents the position along the x-axis.

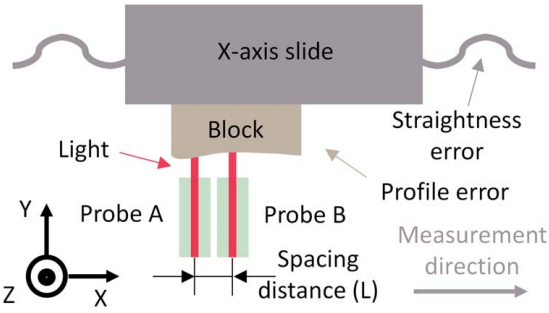

Fig. 2 Setup for STP method

Assuming that $x_n = n \cdot L$, and $n = 0, 1, 2, 3, \ldots, \text{N}$, where L is the spacing distance between two probes, we have:

$$\begin{cases} P_A(x_n) = f(x_n) + e_y(x_n) \\ P_B(x_n) = f(x_n + L) + e_y(x_n) \end{cases} \quad n = 0, 1, 2, 3, \ldots, \text{N} \tag{2}$$

The difference between the two probes' raw outputs can provide the increment of the profile error, and the sum of that increment provides the overall profile error of the standard block. Then, the straightness error can be calculated by removing the profile error. The equation for the separated profile error $f(x)$ and the straightness error $e(x)$ can be expressed by

$$\begin{cases} f(x_n) = \sum_{i=1}^{n} [P_B(x_n) - P_A(x_n)] \\ e_y(x_n) = P_A(x_n) - f(x_n) \end{cases} \quad n = 0, 1, 2, 3, \ldots, \text{N} \tag{3}$$

However, Fig. 2 only shows the ideal condition when the yawing/pitching/rolling error of the slide is not included. Besides that, there are some other errors that need to be considered: the mounting error of the interferometers, the positioning error of the slide, etc. In order to make this method applicable, the analysis of the measurement error needs to be discussed.

3 Measurement Error Analysis

This section mainly explains the slide errors that can influence the precision of the measurement result. The slide has three straightness errors (e_x, e_y, and e_z along x-, y-, and z-directions) and three angular errors. Further, the installation of the sensors can involve assembly errors. The movement of the x-axis for the measurement can lead to a positioning error, e_p. The influence of these errors is discussed in this section.

3.1 System Errors. First, the influence of errors comes from the slide that needs to be investigated. The x- and z-directional straightness errors (e_x and e_z) can deviate the sensors' position and influence the y-directional straightness measurement precision. Besides the straightness error, the angular error of the machine tool can also be converted into the linear error due to its relatively small magnitude [26], which are represented by e_{xa}, e_{ya}, and e_{za} along x-, y-, and z-directions. The y-directional converted linear error, e_{ya}, can contribute to the final y-directional straightness measurement, while e_{xa} and e_{za} can influence the measurement precision.

Further, the assembly error of the optical fibers also needs to be considered. The yawing/pitching/rolling can also be simplified into the linear distance error as mentioned earlier. Then, the mounting error of interferometers can also be divided into the x-, y-, and z-directional linear assembly errors, which are e_{xm}, e_{ym}, and e_{zm}. Here, the x-directional assembly error can directly influence the spacing distance L between two sensors. Since $P_A(x_n)$ and $P_B(x_n)$ from Eq. (2) are sorted from the raw sensors' output according to

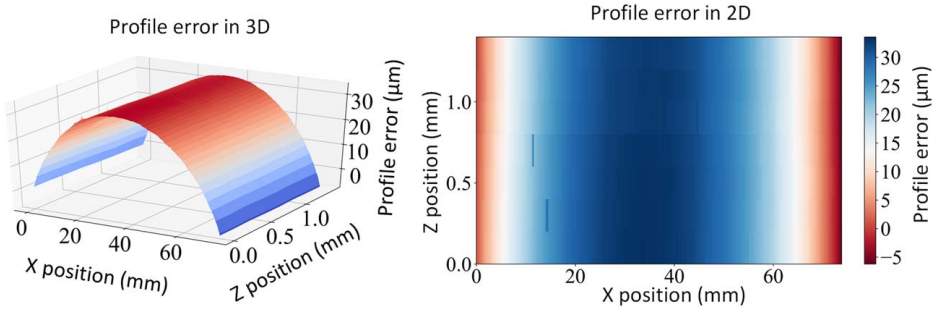

Fig. 3 Profile of the standard block

the spacing distance L, an accurate measurement of the spacing distance needs to be executed to avoid the mismatch of the data points. Since e_{xm} is a fixed value, and the spacing distance with this error can shift the entire measurement data from the target profile to be measured along x-axis, this shifting distance, L', can be calculated by the difference of the centers for the measured profiles

$$L' = L + e_{xm} = \frac{\sum_0^N \overline{P_A}(x_n) \cdot nL}{\sum_0^N \overline{P_A}(x_n)} - \frac{\sum_0^N \overline{P_B}(x_n) \cdot nL}{\sum_0^N \overline{P_B}(x_n)}$$
$$n = 0, 1, 2, 3, \ldots, \mathrm{N} \tag{4}$$

where $\overline{P_A}(x_n)$ and $\overline{P_B}(x_n)$ are averaged sensors' outputs over several measurements to remove the random error. The raw sensor's output usually runs at a high resolution along x-axis, denoted by l, and ideally, the spacing distance L is an integer multiple of l ($L = m \cdot l$, where $m \in \mathrm{N}$) since $P_A(x_n)$ and $P_B(x_n)$ need to be sorted from the sensors' raw output by every m points. However, this e_{xm} can change this relationship and the required data point in the STP method can sometimes be skipped by the sensors' scanning since L' is no more the integer multiple of l. In this condition, we select the closest point from the sensor's raw output, and this can involve another error along the x-axis, denoted by e_s, which can be represented by:

$$e_s = \min(l - nL' \backslash l, \quad nL' \backslash l) \tag{5}$$

The y-directional assembly error, e_{ym}, is another fixed error that can shift the measured data along y-axis. This error can be compensated by the difference of the averages of $\overline{P_A}(x_n)$ and $\overline{P_B}(x_n)$. The assembly error along z-direction, e_{zm}, cannot be compensated which can influence the straightness measurement result.

Last, the x-axis slide also has the positioning error e_p. Then, the total linear errors along x- and z-direction, denoted by $e_{x_{\text{total}}}$ and $e_{z_{\text{total}}}$, can be represented by

$$\begin{cases} e_{x_{\text{total}}} = e_x + e_{xa} + e_{xm} + e_s + e_p \\ e_{z_{\text{total}}} = e_z + e_{za} + e_{zm} \end{cases} \tag{6}$$

3.2 Influence of System Errors. The effect of these linear errors can be evaluated according to the slope of the measured surface. Ideally, if the measured surface profile is pure flat, the deviation along the x- and z-axis cannot influence the y-directional measurement error. However, since the standard block is not pure flat, the slope of the surface profile can convert the error from other directions to the y-directional measurement error. In order to evaluate this effect, the profile of the well-polished standard block has been measured by a precision Hexagon Coordinate Measurement Machine (CMM). We measure an area of 1.4 mm × 75 mm with a spacing distance of 0.2 mm between two measurement points. The final profile error is shown in Fig. 3. It can be seen that the surface profile changes smoothly with a very small slope. The Peak to Valley (PV) value for the entire profile is around 30 μm.

Then, we calculate the gradient of the surface profile along the x-axis and z-axis, respectively, and provide the surface slope. The surface slope along the z-axis is shown in Fig. 4. It can be seen that, ignoring the outliers, the surface slope is around -3 μm to 2 μm per mm, which means for every 1 mm change along the z-axis, the final surface change along the height direction (y-axis according to Fig. 2) can be around -3 μm to 2 μm. Figure 5 shows that for every 1 mm change along the x-axis, the final surface change is less than ± 4 μm.

The positioning error e_p of the slides is usually less than 0.1 mm. The mounting error e_{zm} of the optical fibers can be well adjusted using a dial gauge to reach several microns precision. The e_{xa} and e_{za} is determined by the angular error which is usually less than 0.1 mm magnitude according to specifications of current commercially available machine tools. The error caused by the data selection, e_s, is bounded by the x-axis resolution of the sensors' raw output, which has been selected as 0.05 mm. The magnitude of the overall linear errors along x-axis, $e_{x_{\text{total}}}$, and z-axis, $e_{z_{\text{total}}}$, should be less than 0.5 mm or even close to 0.1 mm, which can cause sub-

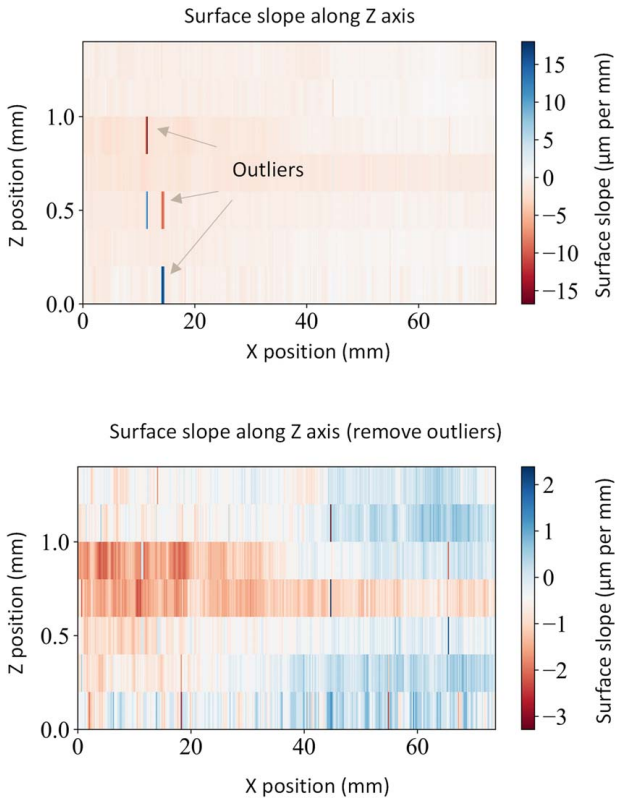

Fig. 4 Surface slope along *y*-axis direction

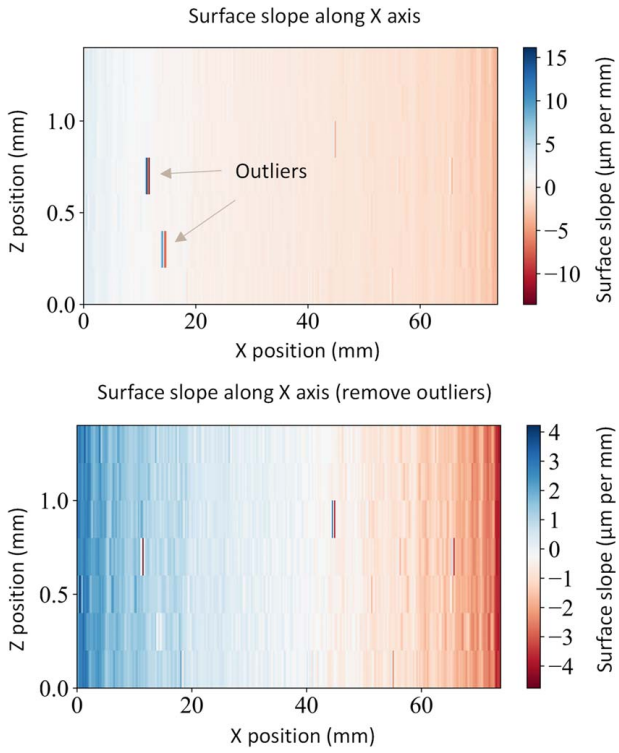

Fig. 5 Surface slope along *x*-axis direction

micron errors in *y*-direction measurement. This error does not influence the final measurement output which can be ignored.

4 Experiment Setup

Figure 6 shows the setup for the on-machine straightness measurement. A commercially available computer numerical control (CNC) machine tool has been used to measure its *x*-axis straightness. The well-polished standard reference block has been fixed on the *x*-axis slide using epoxy with its reference surface facing toward the negative direction of the *y*-axis. The standard block is a commercially available low-cost 1–2–3 block with a squareness of 0.003″ (per inch), a flatness of 0.002″, and a parallelism of 0.002″. The polishing process has been conducted on a low-cost polishing machine while the surface profile has been presented in Sec. 3. Two optical fibers have been mounted on the base of the machine tool using glass ferrules. The glass ferrules and the fiber have been fixed on the glass substrate using ultraviolet (UV)-curable epoxy. The axes of the optical fibers are perpendicular to the reference surface, facing toward the positive direction of *y*-axis. The standard block can move with the *x*-axis slide while the optical fibers are fixed on the machine tool, which can measure the profile of the standard block.

Two optical fibers have been connected to the same interrogator using different channels to capture the wave spectrum of the reflected light. To obtain a proper FSR for our interrogator (1510 nm to 1590 nm) during the experiment, the gap between the tip of the fiber and the reference surface should be maintained within the range of 200–500 μm throughout the experiment. In this experiment, the initial gap has been set as around 300 μm.

The machine tool uses Delta Tau's programmable multi-axis controller (PMAC) to control the position of the *x*-axis. The interrogator and the PMAC motion controller have been connected to the same computer to coordinate the measurement and the machine tool's operation. The optical fibers start to measure the profile of the standard block from the right edge of the block to its left edge while the *x*-axis slide moves from its relative zero coordinate toward the positive direction of the *x*-axis. After every 100 μm jogging distance, the *x*-axis dwells for 5 s for the optical fiber sensors to get 10 measurement results on the same measurement point. We select the value with the maximum multiplicity as the final measurement data to eliminate the influence of the noise and the machine tool's vibration. The final result shows that the minimum multiplicity of one measurement point is more than 5.

5 Results and Discussion

Three measurement experiments have been conducted to validate the effectiveness of this STP method. Three experiments measure the same area which has been scanned by the CMM mentioned in Sec. 2. The raw sensors' outputs are shown in Fig. 7. It can be seen that the sensors' output is relatively smooth with a high-frequency noise whose magnitude is less than ± 1.5 μm on average. The output from one sensor has around 7 μm difference from the other, which is caused by the assembly error e_{ym}, mentioned in Sec. 2. This error can be compensated by calculating the difference of the average value of the entire sensor's output.

In order to evaluate the precision of the output of the optical fiber sensors, an evaluation process that has the same path as the measurements was repeated 22 times. For each specific monitoring point, 10 or 20 spectra were collected without moving the standard block. Therefore, 19,600 points were measured for stability tests in different locations. The standard deviation of the measurement of each point was calculated. Figure 8 shows the distribution of the standard deviation of all the monitored points. Figures 8(*a*) and 8(*b*) show the standard deviation distribution of probe A and probe B, respectively. As we can see, more than 90% of the standard deviation is less than 0.1 μm. Other than 0.0–0.1 μm, most standard deviations locate in 0.2–0.8 μm (5.09% for probe A and 7.61% for probe B). Similarly, from Fig. 8(*c*), which shows the standard deviation of both sensors, 90.63% sampling points have a standard deviation within 0.0 and 0.1 μm. This result outperforms

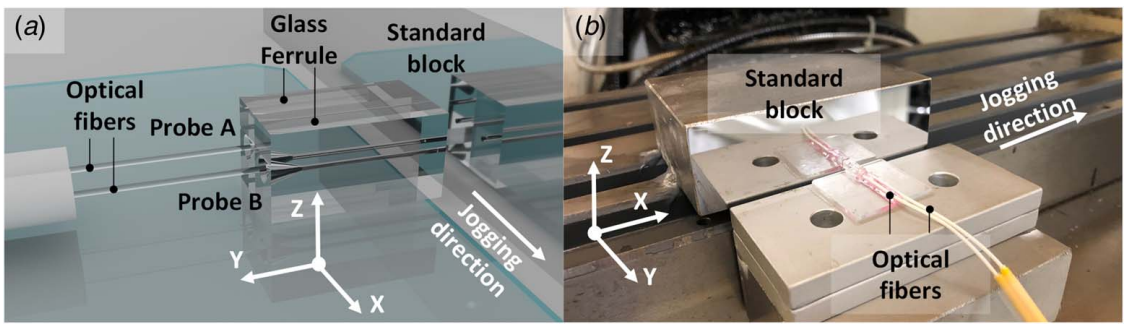

Fig. 6 Setup for STP method. The standard block is mounted on the *x*-axis of the machine tool. Two optical fibers are mounted on the base of the machine tool using glass ferrules, serving as two probes (probes A & B). These two optical fibers can measure the surface of the standard block while the *x*-axis slide jogs toward *x* direction.

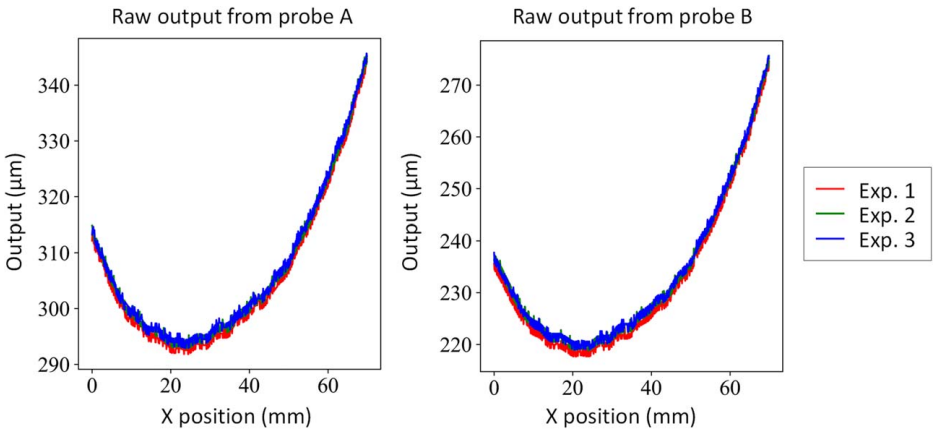

Fig. 7 Raw sensors' output

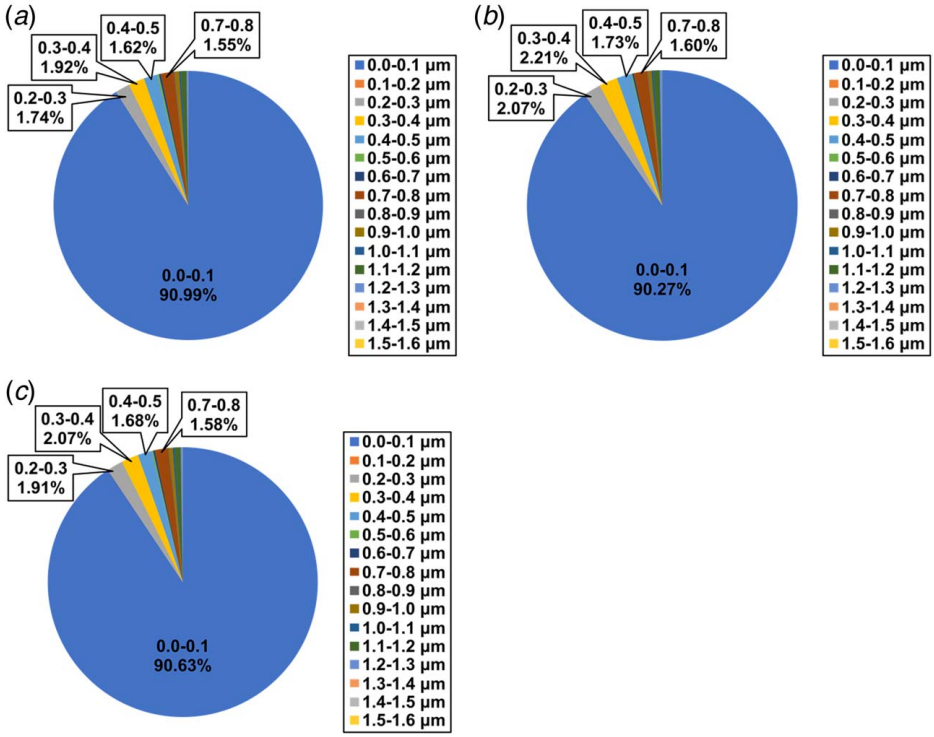

Fig. 8 Distribution of the standard deviations of the evaluation points by percentage: (*a*) probe A, (*b*) probe B, and (c) probe A and probe B

the number of points with a standard deviation higher than 0.1 μm; 98.24% of points have a standard deviation lower than 0.8 μm, and no points have a standard deviation higher than 1.6 μm. Therefore, the optical fiber sensors show excellent precision within our measurement range. Considering the vibration of the CNC machine which may cause slight variation in the distance between the optical fiber and the surface of the standard block, the actual precision can be improved by reducing the vibration.

After compensating for the assembly error, we follow Eq. (3) and separate the profile error and the straightness error, shown in Fig. 9. The real spacing distance between two optical fibers is $L' = 1.5013$ mm, which has been calculated by Eq. (4). In Fig. 9, we compare the separated surface profile result with the profile error measured from CMM. It can be seen that the separated result matches the CMM measurement. The separated straightness error shows that the magnitude of the straightness error in 70 mm range is around 40 μm for our CNC machine tool.

Using CMM measurement result as the standard, we present the measurement error of our STP method in Fig. 10. It can be seen that the measurement data from experiments 2 and 3 have the measurement error of around 2 μm. The first measurement error reaches around 3 μm. This error can come from the alignment error because of the difference between the coordinates from CMM and the machine tool, or the measurement noise. Further, since the STP method calculate the final surface profile by accumulating the increment of the surface shown in Eq. (3), the error can also accumulate in this process. The measurement noise, the vibration of the machine tool, and the surface roughness can all contribute to this error and the small error can be enlarged by this accumulation process. This phenomenon can be represented by the first experiment where the error accumulates at $x = 30$ mm, and this measurement error still exists for the following measurement process till it reaches around 3 μm measurement error when $x = 70$ mm. These noises can be mitigated by a proper low-pass filter, which can improve the overall

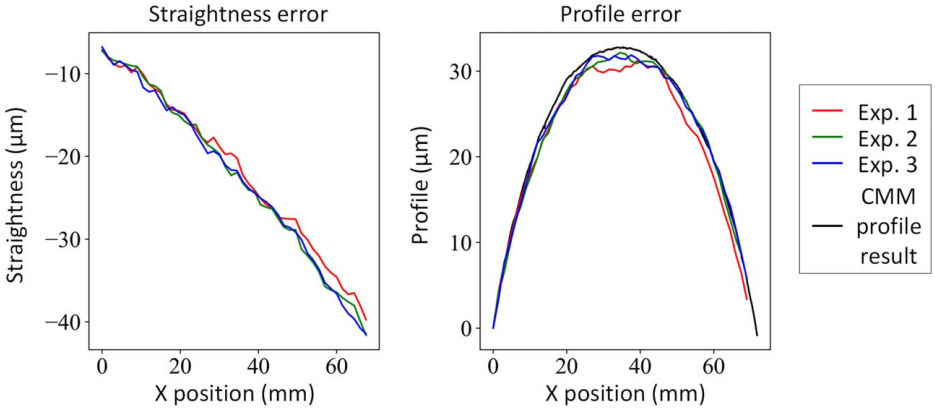

Fig. 9 Separated profile error and straightness error

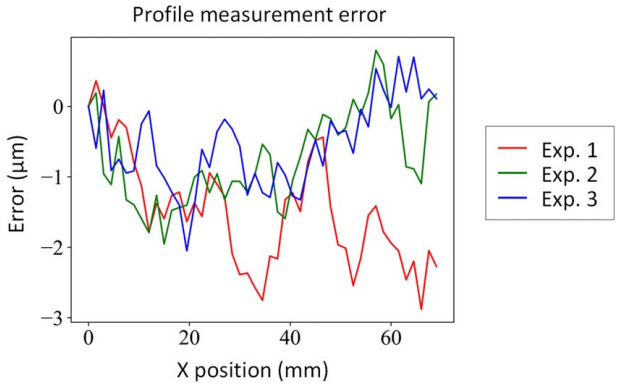

Fig. 10 Separated profile error compared with CMM result

measurement accuracy. However, even without the filter, this STP method can evaluate the straightness error and the profile error with sufficient accuracy.

Though the measurement accuracy cannot be directly evaluated compared with other research since the measurement range, measurement algorithm, machine tool/sensor precision, and measurement setup can all be different, we still provide this comparison to illustrate the advantage of this approach. Compared with the original STP method [27] with the sampling distance of 14.5 mm (that is also the distance between two sensors) with the measurement accuracy of 2 μm on a 363 mm slide, our measurement largely shortens the sampling distance to 1.5 mm with a comparable measurement error on a much shorter measurement interval (70 mm). Compared with the GTP method [26], this method is not highly dependent on the repeatability of the slide to shift the sensor, which can be applied to most commercially available machine tools. Compared with other improved EST methods, for example, those of Refs. [5–7], this method provides a similar micron meter scale measurement error and the result is close to a precision CMM machine. The overall measurement is reliable with high accuracy. Further, the accuracy of one optical fiber sensor is similar to that of the previous method [4–8,11,27], but our interrogator can run up to four optical fiber sensors with only the price of one precision displacement sensor. This large cost saving is also one of the advantages of this method.

6 Conclusion

This paper introduces an F–P interferometer based on-machine straightness error measurement. Two optical fibers have been employed to measure the profile of a well-polished standard block mounting on the x-axis slide. Using the STP method, the y-directional straightness error has been separated from the sensors' output and the profile error of the standard block has been calculated. Compared with the CMM measurement result, the separated profile error has less than 3 μm measurement error, which can verify the precision of this approach. The measured straightness error is around 40 μm in the 70 mm range. This method largely increases the measurement resolution of the EST and has the potential to reach the sub-millimeter scale. The low-cost standard block has been polished by an economical commercially available polishing machine, which is cost-efficient and simple to be applied in industries. This technique can be applied to micro-machine tool's calibration, or some other calibration conditions when only a small range of the slides are used.

It should be noted that the experimental setup shown in Fig. 6 is relatively simple and has a large potential to be commercialized as an industrial product. The fiber bundle with the fixed fiber spacing distance can be assembled into a cable. The STP method applied in this paper employs two fibers, which can only conduct straightness error. However, some other ESTs with more than two sensors can also measure other errors in the slides (for instance, the pitching error using three-point method), which only requires extra input channels from the interrogator. The interrogator that we have used supports 4 input channels and has a comparable price to one precision linear displacement sensor with the same measurement precision. The costs for the optical fiber and the well-polished standard block are relatively negligible. The measurement algorithm can be integrated into the interrogator controller to provide the final separated straightness error and profile error. Therefore, this method provides a potentially alternative cost-efficient approach for the straightness measurement, and it is unique to improve the measurement resolution along the slide moving direction. It has the potential to be improved and applied in the industry in the future.

The limitation of this research is that only a small portion of the x-axis slide has been measured. In future work, the entire straightness error of the slide will be measured using the stitching method. Certain low-pass filters will be applied to remove the influence of the noise.

Acknowledgment

This work was supported in part by the Technology Innovation Program (20015060, Development of Hybrid 3D Printing Machine for Large Scale Additive Manufacturing and Machining Process of CFRP Lightweight Parts) funded By the Ministry of Trade, Industry & Energy (MOTIE, Korea). This work was also supported in part by the Clean Energy Smart Manufacturing Innovation Institute (CESMII) funded by the US Department of Energy (DOE Federal Award No: DE-EE0007613).

Conflict of Interest

There are no conflicts of interest.

Data Availability Statement

The authors attest that all data for this study are included in the paper.

References

[1] Chen, B., Xu, B., Yan, L., Zhang, E., and Liu, Y., 2015, "Laser Straightness Interferometer System With Rotational Error Compensation and Simultaneous Measurement of Six Degrees of Freedom Error Parameters," Opt. Express, **23**(7), pp. 9052–9073.

[2] Whitehouse, D. J., 1976, "Some Theoretical Aspects of Error Separation Techniques in Surface Metrology," J. Phys. E, **9**(7), pp. 531–536.

[3] Tozawa, K., Sato, H., and O-hori, M., 1982, "A New Method for the Measurement of the Straightness of Machine Tools and Machined Work," ASME J. Mech. Des., 104(3), pp. 587–592.

[4] Kiyono, S., and Gao, W., 1994, "Profile Measurement of Machined Surface With a New Differential Method," Precis. Eng., **16**(3), pp. 212–218.

[5] Yin, Z. Q., and Li, S. Y., 2006, "High Accuracy Error Separation Technique for On-Machine Measuring Straightness," Precis. Eng., **30**(2), pp. 192–200.

[6] Su, H., Hong, M. S., Li, Z. J., Wei, Y. L., and Xiong, S. B., 2002, "The Error Analysis and Online Measurement of Linear Slide Motion Error in Machine Tools," Meas. Sci. Technol., **13**(6), pp. 895–902.

[7] Fung, E. H. K., and Yang, S. M., 2000, "An Error Separation Technique for Measuring Straightness Motion Error of a Linear Slide," Meas. Sci. Technol., **11**(10), pp. 1515–1521.

[8] Kiyono, S., 1988, "Erratum to : Study on Measurement of Surface Undulation (2nd Report)," J. Jpn. Soc. Precis. Eng., **54**(5), pp. 976–976.

[9] Omar, B. A., Holloway, A. J., and Emmony, D. C., 1990, "Differential Phase Quadrature Surface Profiling Interferometer," Appl. Opt., **29**(31), p. 4715.

[10] Yin, Z. Q., and Li, S. Y., 2005, "Exact Straightness Reconstruction for On-Machine Measuring Precision Workpiece," Precis. Eng., **29**(4), pp. 456–466.

[11] Gao, W., and Kiyono, S., 1997, "On-Machine Profile Measurement of Machined Surface Using the Combined Three-Point Method," JSME Int. J. Ser. C: Dyn., Control, Rob., Des. Manuf., **40**(2), pp. 253–259.

[12] Shimizu, H., Yamashita, R., Hashiguchi, T., Miyata, T., and Tamaru, Y., 2018, "Square Layout Four-Point Method for Two-Dimensional Profile Measurement and Self-Calibration Method of Zero-Adjustment Error," Int. J. Autom. Technol, **12**(5), pp. 707–713.

[13] Fung, E. H. K., Zhu, M., Zhang, X. Z., and Wong, W. O., 2014, "A Novel Fourier-Eight-Sensor (F8S) Method for Separating Straightness, Yawing and Rolling Motion Errors of a Linear Slide," Measurement (Lond.), **47**(1), pp. 777–788.

[14] Leal-Junior, A. G., Marques, C., Frizera, A., and Pontes, M. J., 2018, "Multi-Interface Level in Oil Tanks and Applications of Optical Fiber Sensors," Opt. Fiber Technol., **40**, pp. 82–92.

[15] Bremer, K., Weigand, F., Zheng, Y., Alwis, L. S., Helbig, R., and Roth, B., 2017, "Structural Health Monitoring Using Textile Reinforcement Structures With Integrated Optical Fiber Sensors," Sensors, **17**(2), p. 345.

[16] Miah, K., and Potter, D. K., 2017, "A Review of Hybrid Fiber-Optic Distributed Simultaneous Vibration and Temperature Sensing Technology and Its Geophysical Applications," Sensors, **17**(11), p. 2511.

[17] Zhou, F., Kung, P., Li, X., Behjat, V., and Jun, M. B. G., 2021, "Modeling of a Sampled Apodized Fiber Bragg Grating Moisture Sensor," Opt. Fiber Technol., **65**, p. 102630.

[18] Wang, X., and Wolfbeis, O. S., 2019, "Fiber-Optic Chemical Sensors and Biosensors (2015–2019)," Anal. Chem., **92**(1), pp. 397–430.

[19] Gupta, B. D., and Kant, R., 2018, "Recent Advances in Surface Plasmon Resonance Based Fiber Optic Chemical and Biosensors Utilizing Bulk and Nanostructures," Opt. Laser Technol., **101**, pp. 144–161.

[20] Gandhi, M. S., Chu, S., Senthilnathan, K., Babu, P. R., Nakkeeran, K., and Li, Q., 2019, "Recent Advances in Plasmonic Sensor-Based Fiber Optic Probes for Biological Applications," Appl. Sci., **9**(5), p. 949.

[21] Zhou, F., Su, H., Joe, H.-E., and Jun, M. B.-G., 2020, "Temperature Insensitive Fiber Optical Refractive Index Probe With Large Dynamic Range at 1,550 nm," Sens. Actuators, A, **312**, p. 112102.

[22] Brambilla, G., Finazzi, V., and Richardson, D. J., 2004, "Ultra-Low-Loss Optical Fiber Nanotapers," Opt. Express, **12**(10), pp. 2258–2263.

[23] Ward, J. M., O'Shea, D. G., Shortt, B. J., Morrissey, M. J., Deasy, K., and Nic Chormaic, S. G., 2006, "Heat-and-Pull Rig for Fiber Taper Fabrication," Rev. Sci. Instrum., **77**(8), p. 83105.

[24] Xue, S., van Eijkelenborg, M. A., Barton, G. W., and Hambley, P., 2007, "Theoretical, Numerical, and Experimental Analysis of Optical Fiber Tapering," J. Lightwave Technol., **25**(5), pp. 1169–1176.

[25] Zhou, F., Duan, W., Li, X., Tsai, J.-T., and Jun, M. B. G., 2021, "High Precision In-Situ Monitoring of Electrochemical Machining Process Using an Optical Fiber Fabry–Pérot Interferometer Sensor," J. Manuf. Process., **68**, pp. 180–188.

[26] Fu, X., Bing, G., Zhao, Q., Rao, Z., Cheng, K., and Mulenga, K., 2016, "Improved Error Separation Technique for On-Machine Optical Lens Measurement," Meas. Sci. Technol., **27**(4), p. 45005.

[27] Tozawa, K., Sato, H., and O-Hori, M., 1982, "A New Method for the Measurement of the Straightness of Machine Tools and Machined Work," ASME J. Mech. Des., **104**(3), pp. 587–592.